Biomaterials 209 (2019) 103–110

Contents lists available at ScienceDirect

Biomaterials

journal homepage: www.elsevier.com/locate/biomaterials

Unique arrangement of bone matrix orthogonal to osteoblast alignment controlled by *Tspan11*-mediated focal adhesion assembly

Yohei Nakanishi[a,1], Aira Matsugaki[a,1], Kosuke Kawahara[b], Takafumi Ninomiya[b], Hiroshi Sawada[b], Takayoshi Nakano[a,*]

[a] Division of Materials and Manufacturing Science, Graduate School of Engineering, Osaka University, Osaka 2-1 Yamada-oka, Suita, Osaka, 565-0871, Japan
[b] Canon Machinery Inc., Shiga 85 Minami Yamada-cho, Kusatsu, Shiga, 525-8511, Japan

ARTICLE INFO

Keywords:
Osteoblast
Focal adhesion
Bone matrix
Tspan11
Cell orientation

ABSTRACT

During tissue construction, cells coordinate extracellular matrix (ECM) assembly depending on the cellular arrangement. The traditional understanding of the relationship between the ECM and cells is limited to the orientation-matched interaction between them. Indeed, it is commonly accepted that the bone matrix (collagen/apatite) is formed along osteoblast orientation. Nonetheless, our recent findings are contrary to the above theory; osteoblasts on nanogrooves organize formation of the bone matrix perpendicular to cell orientation. However, the precise molecular mechanisms underlying the orthogonal organization of bone matrix are still unknown. Here, we show that mature fibrillar focal adhesions (FAs) facilitate the perpendicular arrangement between cells and bone matrix. The osteoblasts aligned along nanogrooves expressed highly mature fibrillar FAs mediated by integrin clustering. Microarray analysis revealed that *Tspan11*, a member of the transmembrane tetraspanin protein family, was upregulated in cells on the nanogrooved surface compared with that in cells on isotropic, flat, or rough surfaces. *Tspan11* silencing significantly disrupted osteoblast alignment and further construction of aligned bone matrix orthogonal to cell orientation. Our results demonstrate that the unique bone matrix formation orthogonal to cell alignment is facilitated by FA maturation. To the best of our knowledge, this report is the first to show that FA assembly mediated by *Tspan11* determines the direction of bone matrix organization.

1. Introduction

The ability of cells to sense and align in response to the surroundings is essential for multicellular matrix formation with appropriate architecture in both the developmental stage and regeneration processes. In particular, the characteristic texture of bone tissue derived from collagen/apatite [1–3] is determined by the osteoblast directional behaviors [4,5]. We have clarified that osteoblasts produce bone matrix along cell alignment; even the crystallographic texture of apatite is regulated by the degree of cell alignment [6]. On the other hand, our recent work surprisingly unveiled a quite unique phenomenon characterized by the construction of bone matrix orthogonal to osteoblast alignment, which was induced by a nanogrooved structure [7]. This finding challenges the classical belief that the cell-produced matrix orientation follows the cellular direction in extracellular matrix (ECM) assembly [8–10]. It is expected that cells contain intrinsic molecular regulatory systems determining parallel or perpendicular bone matrix construction in response to the substrates surface.

Cellular recognition of the substrate surface is mediated by focal adhesions (FAs), which are assembled multiprotein structures that include transmembrane receptor integrin, which is composed of nanoscale head and tail structure [11]. FA formation is controlled by the integrin clustering procedure mediated by multiple associated proteins [12]. The function of FAs is regulated by the dynamic maturation process in which FAs undergo morphological and compositional change driven by cellular tension; FA maturation proceeds to the formation of fibrillar FAs, which are responsible for the structural regulation of the ECM [13].

The aim of the present study is to clarify a molecular mechanism underlying our previous finding of cellular organization of bone matrix orthogonal to cell alignment [7]. Here, we focused on the morphological change of FAs as well as the cellular alignment in response to nanoscale geometry. Specifically, the osteoblasts aligned along the nanogrooves expressed supermature fibrillar FAs. Moreover, comprehensive microarray analysis enabled the identification of genetic cues triggering the uniquely oriented bone matrix formation. The identified

* Corresponding author.
E-mail address: nakano@mat.eng.osaka-u.ac.jp (T. Nakano).
[1] These authors contributed equally to this work.

https://doi.org/10.1016/j.biomaterials.2019.04.016
Received 9 October 2018; Received in revised form 10 April 2019; Accepted 11 April 2019
Available online 16 April 2019

Tspan11 significantly contributed to the perpendicular bone matrix construction by regulating the integrin clustering. The present findings of molecular regulatory systems for anisotropic bone matrix formation may lead to the development of novel biomaterials and therapeutic targets for recovery of healthy bone with appropriate matrix alignment.

2. Materials and methods

2.1. Fabrication and characterization of surface structures

Ti-6 mass% Al-4 mass% V alloy (Ti-6Al-4V; ASTM F136-08) with a diameter of 13 mm and a height of 5.0 mm was prepared. After ground by emery paper (#600), the material surface was polished using diamond paste (grain size, 9 and 3 μm) and colloidal silica suspension (grain size, 0.06 μm). On these samples, a nanogrooved structure was fabricated using a p-polarized Ti:sapphire femtosecond laser (peak wavelength of 800 nm, pulse width of 250 fs, cyclic frequency of 2 kHz). As a control substrate, a non-directional rough structure was generated using a circularly polarized laser. In order to clarify the effect of surface roughness, a flat surface was also prepared by polishing with the initial preparation procedure. The resulting surface topography of each substrate was observed and analyzed quantitatively with a scanning probe microscope (SPM; Nanocute, Hitachi High-Tech Science, Tokyo, Japan). The surface roughness Ra (arithmetic average height) was determined as the average absolute deviation of the roughness irregularities from the mean line within a 13 μm × 13 μm area of separated 5 regions for each sample.

2.2. Isolation and culture of osteoblasts

Primary osteoblasts were isolated from the calvariae of newborn C57BL/6 mice (3 days old) by sequential enzymatic treatment with collagenase/trypsin (collagenase: Wako, Osaka, Japan; trypsin: Nacalai Tesque, Kyoto, Japan). In a sterile environment, the calvariae were extracted, and the tissues surrounding the calvariae were removed in α-modified Eagle's medium (α-MEM; Gibco, Grand Island, NY, USA). After washing with Hanks' balanced salt solution (HBSS; Gibco), the calvariae were treated with collagenase/trypsin five times at 37 °C for 15 min each. The supernatants of the first two treatments were discarded, and the supernatants of the third, fourth, and fifth treatments were collected with α-MEM. Following filtration with a 100-μm mesh strainer (BD Biosciences, San Jose, CA, USA) and centrifugation, the accumulated cells were suspended in α-MEM with 10% fetal bovine serum (FBS; Gibco) and 1% penicillin and streptomycin (Invitrogen, Carlsbad, CA, USA). All animal experiments were approved by the Osaka University Committee for Animal Experimentation.

Isolated osteoblasts were seeded onto each substrate at a density of 8000 cells/cm^2. The cells were incubated at 37 °C in 5% CO_2, and medium was changed twice a week. For mineralization induction, after culturing for 1 week, the medium was supplemented with 50 μg/mL ascorbic acid (Sigma, St. Louis, MO, USA), 10 mM β-glycerophosphate (Tokyo Kasei, Tokyo, Japan), and 50 nM dexamethasone (MP Bioscience, Solon, OH, USA) at final concentrations.

2.3. Short-term silencing of Tspan11

Small interfering RNA (siRNA)-mediated knockdown was performed using electroporation (Neon Transfection System, Invitrogen). *Tspan11*-specific SMARTpool siRNAs (no. M-058535-01; Dharmacon, Lafayette, CO, USA) were used at a final concentration of 100 nM to silence *Tspan11*. A non-targeting siRNA pool was used as the control (no. D-001206-13; Dharmacon). The cells transfected with *Tspan11* siRNA and control siRNA were seeded onto the fabricated substrates at a density of 8000 cells/cm^2 and cultured for 24 h.

2.4. Long-term silencing of Tspan11

For long-term gene silencing in cultured osteoblasts (4 weeks), Accell siRNA (no. E-058535-00; Dharmacon) was applied to induce *Tspan11* knockdown according to the manufacturer's protocol. The Accell non-targeting pool was applied as the control (no. D-001910-10; Dharmacon). Following the initial culture in normal growth medium (α-MEM with 10% FBS and 1% penicillin and streptomycin) for 24 h, cells were treated with Accell siRNA resuspended in the Accell delivery media (Dharmacon). After 72-h culture, the delivery medium was replaced with normal growth medium. The above procedure was repeated for 4 weeks of cultivation.

2.5. Immunofluorescence staining

After 24-h culture, cells on the substrates were fixed with 4% formaldehyde in phosphate-buffered saline (PBS) for 20 min. After washing with PBST (PBS containing 0.05% Triton X-100), cells were blocked with PBST containing 1% normal goat serum (NGS; Invitrogen) for 30 min. For immunostaining of vinculins, the cells were incubated with mouse monoclonal antibodies against vinculin (Sigma-Aldrich) at 4 °C overnight. After rinsing with PBS, the cells were treated with secondary antibodies (Alexa Fluor 546-conjugated anti-mouse IgG, Invitrogen) and DAPI (Invitrogen) and incubated at room temperature for 2 h. For visualization of F-actin, the cells were treated with Alexa Fluor 488-conjugated phalloidin (Invitrogen). At last, the cells were washed with PBST and mounted in Prolong Gold antifade reagent (Invitrogen). The samples were observed under a fluorescence microscope (BZ-X710, Keyence, Osaka, Japan).

To visualize collagen fibers, the cells and collagen matrices were fixed after 2 weeks of culture. Rabbit polyclonal antibodies against collagen type I (Abcam, Cambridge, MA, USA) were applied as described earlier in this section.

2.6. Morphological analysis of cells and FAs

Morphological features of cells were quantitatively analyzed based on phalloidin staining images. Photographs of fluorescent stain captured by fluorescence microscopy were binarized using Adobe Photoshop CS3 software and analyzed using Cell Profiler software (Broad Institute, Cambridge, MA, USA). The degree of cell orientation, f_{2D}, was determined by the following equations [14]:

$$f_{2D} = 2(<\cos^2\theta> - 0.5)$$

$$<\cos^2\theta> = \left(\sum_1^n \cos^2\theta\right)/n$$

Inclusion criteria for cell analysis were as follows: cells with no cell–cell contact and cells of 500-μm^2 size or larger.

For morphological analysis of FAs, vinculin staining images were processed and analyzed as described earlier in this section using Adobe Photoshop CS3 software and Cell Profiler software. In this analysis, FAs were detected as bright clusters of vinculin. The aspect ratio of FAs was determined by the ratio of the major axis to the minor axis. In addition, the degree of cell alignment in Fig. 5C was calculated by the difference in the appearance frequency between 0° (± 10°) and 90° (± 10°).

2.7. Raman microscopic analysis

After 4 weeks of culture on the substrates, the orientation of collagen matrices secreted by the osteoblasts was analyzed using Raman microscopy (NRS-5100, JASCO, Tokyo, Japan). Collagen shows exceptional optical characteristics derived from its fibril alignment, which enable to extract the aligned properties of collagen matrices by rotating the polarization direction of incident laser [15]. The orientation of collagen matrices can be identified by focusing on the intensity of

amide I (~1664 cm^{-1}) and C—H bending (~1451 cm^{-1}) Raman bands. The intensity of amide I (C═O bonds) depends on the orientation of collagen molecules, since C═O bonds are oriented perpendicular to the backbone of collagen molecules. On the other hand, C—H bonds have no preferential orientation to the backbone of collagen molecules. Accordingly, the orientation of collagen matrices can be identified by the intensity ratio of amide I to C—H bending (ν(C═O)/δ(C—H)). To determine the orientation of collagen matrices secreted on the substrates, the intensity ratio was measured at every 10° by rotating the samples 360° with respect to the polarization of the incident laser beam. The point where the laser polarization direction was consistent with the nanogrooved direction was set as the starting point (0°). In addition, the degree of collagen orientation in Fig. 5C was calculated by the difference in the intensity ratio between 0° (±10°) and 90° (±10°).

2.8. Microarray analysis

Comprehensive gene expression profiles of osteoblasts were analyzed after 4 weeks of culture on each substrate. Total RNA of the cells was extracted using NucleoSpin RNA XS (Macherey-Nagel GmbH & Co, Düren, Germany). To test for quality, the RNA purity and integrity were evaluated by the Agilent 2100 Bioanalyzer (Agilent Technologies, Santa Clara, CA, USA). The fragmentation and labeling of cDNA were performed according to the Affymetrix GeneChip Expression Analysis Manual. The obtained samples were then hybridized to the Affymetrix GeneChip Mouse Gene 2.0 ST Array (Santa Clara, CA, USA). The arrays were scanned and processed according to the manufacturer's specifications.

2.9. Statistical analysis

Values are reported as the mean ± standard deviation (SD). Statistical significance between two groups was tested using the Student's *t*-test or Welch's *t*-test. For comparison between three groups, one-way analysis of variance (ANOVA) was conducted followed by Tukey's multiple comparison tests. Significance was established when $p < 0.05$ and $p < 0.01$.

3. Results

3.1. Characterization of surface structure

SPM images revealed that the two different types of surface topography (rough and nanogrooved) were successfully induced on the Ti-6Al-4V alloy surface by irradiation of femtosecond laser. On the other hand, the smooth, flat surface was obtained by mirror surface grinding (Fig. 1). Quantitative analysis with SPM showed that the nanogrooved structure had a pitch of 579 ± 21 nm and a depth of 168 ± 6 nm, whereas the flat surface had lower surface roughness than the nanogrooved and rough surfaces.

3.2. Effects of surface topography on cell adhesion

Osteoblasts showed specific responses depending on the substrate topography. Immunofluorescence staining images revealed that osteoblasts cultured on the nanogrooved surface were highly elongated and aligned along the nanogroove. In contrast, osteoblasts cultured on the rough and flat surfaces spread randomly. The distribution of cell orientation on each substrate was shown in histograms (Fig. 2A). Quantitative analysis revealed that the degree of cell alignment was specifically higher in cells cultured on the nanogrooved surface, whereas the cells cultured on the rough and flat surfaces exhibited non-directional alignment (Fig. 2B). On the other hand, the cell area of osteoblasts cultured on the flat surface was much higher than that of osteoblasts cultured on the nanogrooved and rough surfaces.

3.3. FA formation in response to surface topography

Fluorescence staining images showed that FAs on the nanogrooved surface were mainly oriented in the nanogroove direction, whereas FAs on the rough and flat surfaces were oriented randomly (Fig. 2C). Quantitative analysis revealed that the ratio of aligned FAs was much higher on the nanogrooved surface than on the rough and flat surfaces. It was also observed that FAs oriented in the groove direction were highly elongated, and the aspect ratio of aligned FAs was higher on the nanogrooved surface as indicated by quantitative analysis. On the other hand, cells cultured on the flat surface had higher numbers of FAs.

3.4. Bone matrix organization

The collagen matrix deposited by the cells aligned along the nanogrooved surface showed preferred alignment orthogonal to cell direction (Fig. 3A). In contrast, collagen matrix that was secreted on the rough and flat surfaces showed random orientation. The preferred orientation of collagen matrices was quantitatively evaluated using Raman microscopic analysis. In the case of the nanogrooved surface, the intensity ratio of ν(C═O)/δ(C—H) was high when the direction of laser polarization was consistent with that of the nanogrooved structure (at rotation angles of 0° and 180°). This indicates that C═O bonds were aligned along the nanogrooves, and collagen matrices were aligned orthogonal to the nanogroove direction. On the contrary, the intensity ratio showed almost the same value at all directions in the case of the rough and flat surfaces, indicating that the collagen matrices showed non-directional orientation (Fig. 3B).

3.5. Gene expression profiles depending on the surface topography

Gene expression levels of osteoblasts cultured on flat, rough, or nanogrooved surfaces were compared. The numbers of increased and decreased transcripts depending on the surface topography were represented in a Venn diagram (Fig. 4). The up- and downregulation of multiple genes were driven by surface topography. Common genes significantly altered in osteoblasts cultured on the nanogrooved or flat

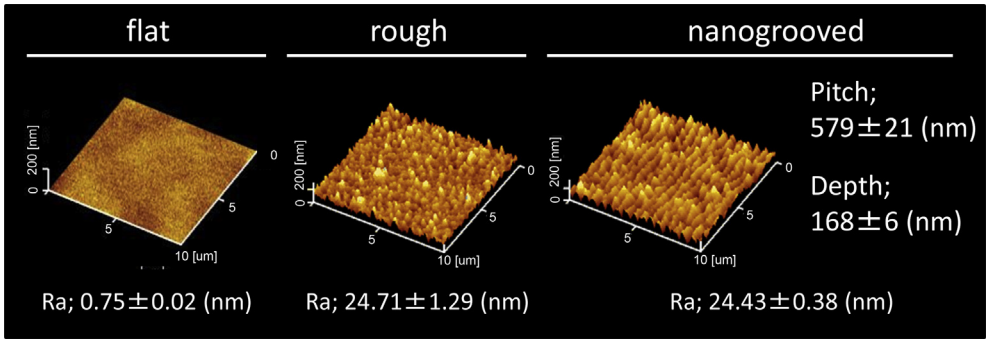

Fig. 1. SPM images of the fabricated surface topography. (Left) A flat surface was prepared by mirror polishing, and (middle) a rough surface was fabricated using irradiation of a circularly polarized laser. (Right) A nanogrooved structure with a pitch of approximately 580 nm and depth of 170 nm was fabricated by irradiation of a p-polarized femtosecond laser. The value of corresponding surface roughness (Ra) is indicated below the images.

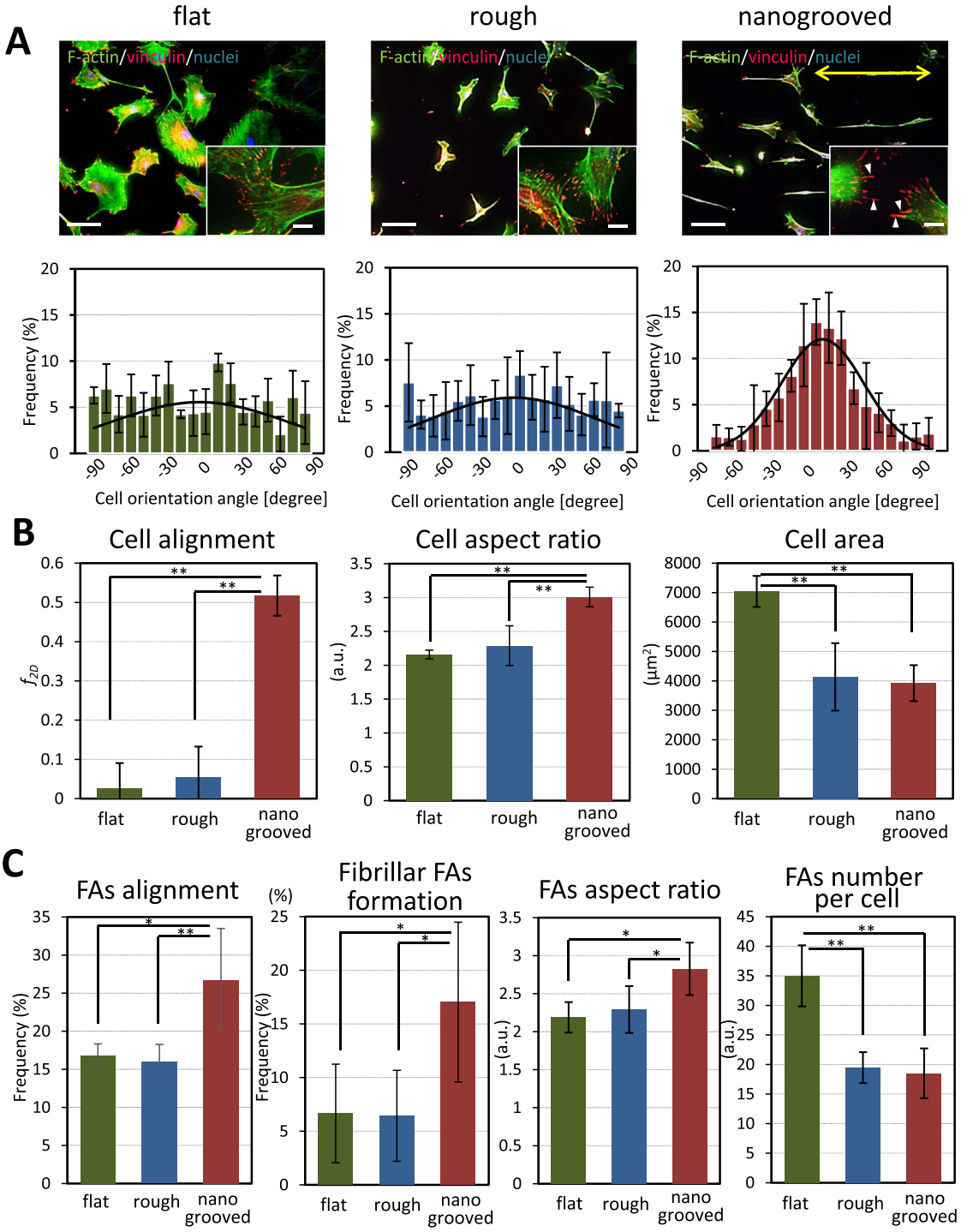

Fig. 2. A. Immunofluorescence images and the distribution of osteoblast orientation on each substrate. Scale bars, 100 μm. Doubled-headed yellow arrow indicates the direction of nanogrooves. The insets show magnified images of FAs on each substrate. Scale bars, 20 μm. **B.** Quantitative analysis of cell morphological parameters; degree of cell alignment (f_{2D}), cell aspect ratio, and cell area. **C.** Quantitative analysis of FA morphological parameters; frequency of aligned (concentrated between −10° and 10° against groove direction) FAs, formation of fibrillar FAs (> 5 μm), FA aspect ratio, and FA number per single cell.*; $P < 0.05$, **; $P < 0.01$. (For interpretation of the references to colour in this figure legend, the reader is referred to the Web version of this article.)

surfaces were identified. Among them, annotated genes encoding cell adhesion-related molecules were identified; *Tspan11* and *Gpm6b* were particularly enriched in osteoblasts aligned on the nanogrooved and flat surfaces, respectively.

3.6. Effect of Tspan11 silencing on bone matrix orientation

Tspan11-silenced osteoblasts failed to align along the nanogrooved surface at the intact level; the degree of cell alignment was significantly lower compared with that of control osteoblasts (Fig. 5A), indicating that *Tspan11* plays key roles in controlling cell alignment induced by nanoscale surface topography. The effects of *Tspan11* silencing on anisotropic bone matrix organization were further investigated by long-term gene silencing using Accell siRNA transfection. The quantitative analysis with Raman microscopy revealed that the collagen matrix alignment orthogonal to osteoblast arrangement was significantly

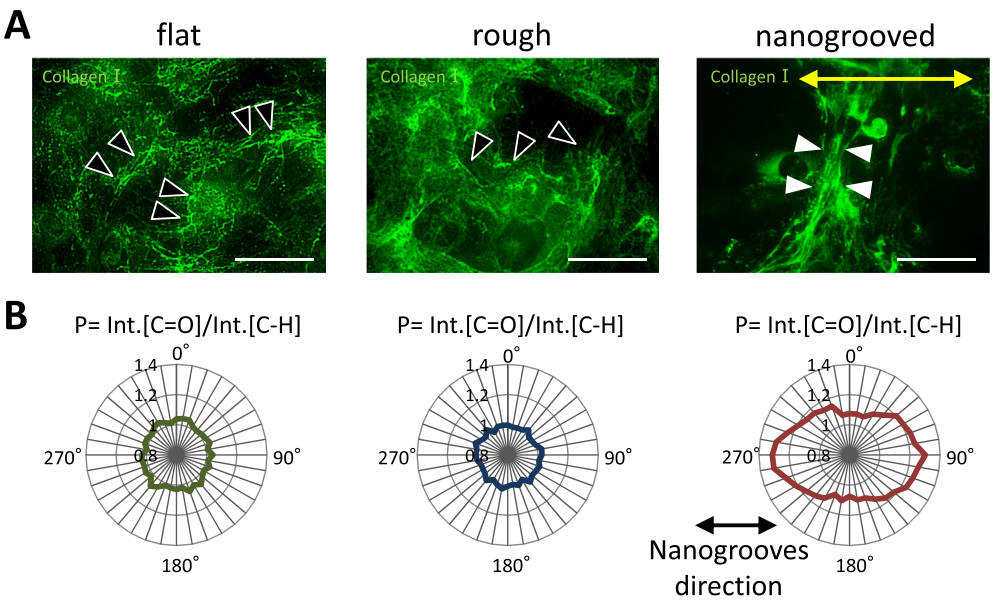

Fig. 3. A. Immunofluorescence images of cell-produced collagen matrix. Scale bars, 100 μm. Doubled-headed yellow arrow indicates the direction of nanogrooves. **B.** Quantitative analysis of collagen matrix orientation using Raman microscopy, calculated by the intensity ratio of ν(C═O)/δ(C−H). The analysis was performed by rotating the samples 360° against the laser polarization direction. Doubled-headed black arrow indicates the direction of nanogrooves. (For interpretation of the references to colour in this figure legend, the reader is referred to the Web version of this article.)

disrupted by *Tspan11* silencing (Fig. 5B). The degree of disruption in cell alignment along nanogrooves and collagen matrix orientation perpendicular to nanogrooves induced by *Tspan11* silencing was compared. The obtained results indicated that *Tspan11* regulates osteoblast alignment and further orientation of bone matrix formation in a direction perpendicular to the cells (Fig. 5C).

4. Discussion

In this study, we firstly demonstrated that the abnormal arrangement of bone matrix orthogonal to osteoblast alignment was regulated via a cell adhesion-mediated pathway. The present study revealed that bone matrix organization orthogonal to osteoblast alignment is characterized by highly elongated mature FA formation mediated by the function of *Tspan11* along the nanogroove direction.

4.1. Surface structure introduced by laser irradiation

Flat, rough, and nanogrooved structures were successfully introduced on Ti-6Al-4V alloy surface. The rough and nanogrooved structures showed comparable surface roughness, whereas the flat surface obtained by mirror finish demonstrated extremely low values of surface roughness (Fig. 1). The comparison between flat and rough surfaces indicated that the surface roughness affected cell behaviors, and the comparison between rough and nanogrooved surfaces enabled analysis of the effects of grating structure on cell behavior. The obtained nanogrooved structure had a pitch smaller than the wavelength of the incident laser, consistent with a previous report [16].

4.2. Osteoblast response to surface topography

Osteoblast adhesion behaviors were clearly affected by the surface patterning. Osteoblasts were highly elongated and aligned along the nanogrooves (Fig. 2). Cellular sensing and responses to nanoscale patterning are determined by cell adhesion processes mediated by filopodia [17] and lamellipodia [18]. The molecular architecture of these cytoskeletal structures is mediated by FA growth, which plays an important role as a mechanical link between surface structures and the cytoskeleton [19]. Mature, elongated FA structure along the nanogrooved surface was observed in this study and correlated with the direction of cell elongation. The forces applied to FAs affect the cytoskeletal organization, which in turn affects the whole-cell alignment along nanogrooves. Indeed, Natale et al. have clarified the nanoconfinement of FAs, i.e., FAs aligned along the nanogrooves induce cell alignment along the nanogrooves [20].

Osteoblasts cultured on the flat surface showed an enlarged cell area

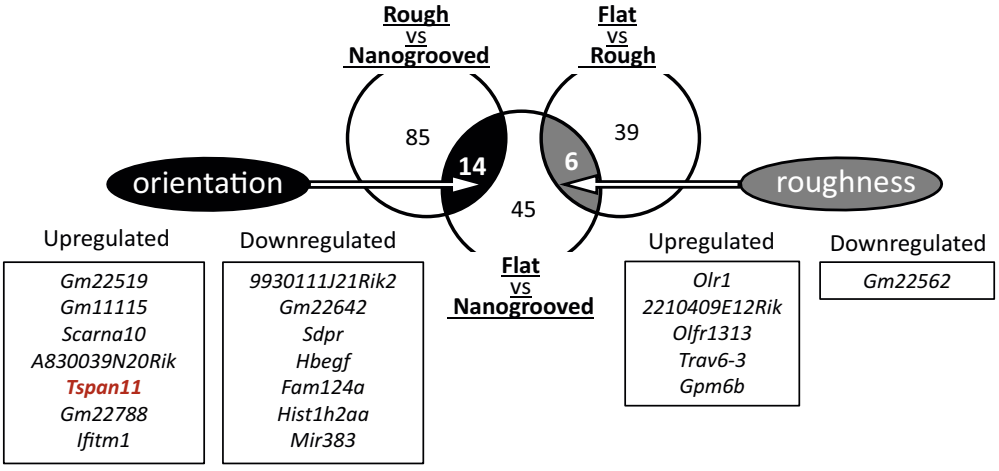

Fig. 4. Venn diagram of microarray gene expression analysis. The comparison of differentially expressed genes between each substrate (> 1.5-fold).

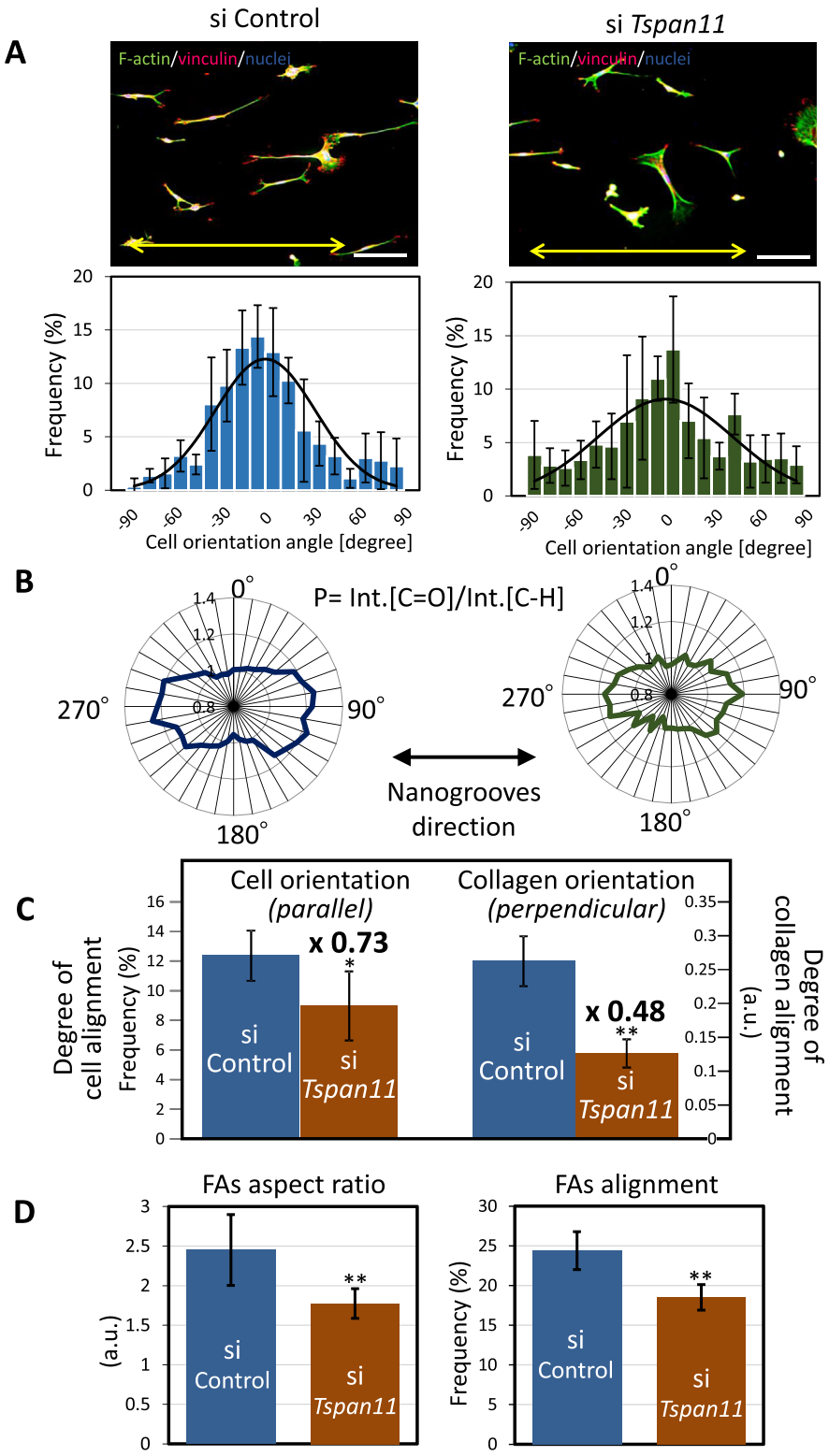

Fig. 5. A. Immunofluorescence images and the distribution of cell orientation of control osteoblasts and *Tspan11*-silenced osteoblasts on the nanogrooved surface. Scale bars, 100 μm. Doubled-headed yellow arrows indicate the direction of nanogrooves. B. Quantitative analysis of collagen matrix orientation using Raman microscopy, calculated by the intensity ratio of ν(C═O)/δ(C−H). The degree of collagen matrix alignment was calculated by P [0°]–P [90°]. C. Comparison of the degree of disruption in alignment between cells (parallel to nanogrooves) and collagen matrix (perpendicular to nanogrooves). D. Quantitative analysis of FA morphology of control and *Tspan11*-silenced osteoblasts.*; $P < 0.05$, **; $P < 0.01$. (For interpretation of the references to colour in this figure legend, the reader is referred to the Web version of this article.)

compared with those cultured on rough or nanogrooved surfaces (Fig. 2). These widespread osteoblasts on the flat surface expressed a significantly increased number of FAs per single cell. Laser-induced surface modification altered the titanium surface hydrophilicity and protein adsorption behaviors on the surface. The flat mirror surface provided abundant cell adhesion sites and resulted in the stabilization of cell adhesion [21]. Moreover, gene expression analysis revealed six candidate genes (*Gm22562*, *Olr1*, *2210409E12Rik*, *Olfr1313*, *Trav6-3*, and *Gpm6b*) that control cellular response to surface roughness (Fig. 4). For example, *Gpm6b* (glycoprotein m6b) was significantly upregulated in the cells cultured on the flat surface. GPM6B is a transmembrane protein that belongs to the proteolipid protein family. A previous study reported that *Gpm6b* regulates several osteoblast functions and, in particular, is involved in cytoskeletal organization [22]. The obtained

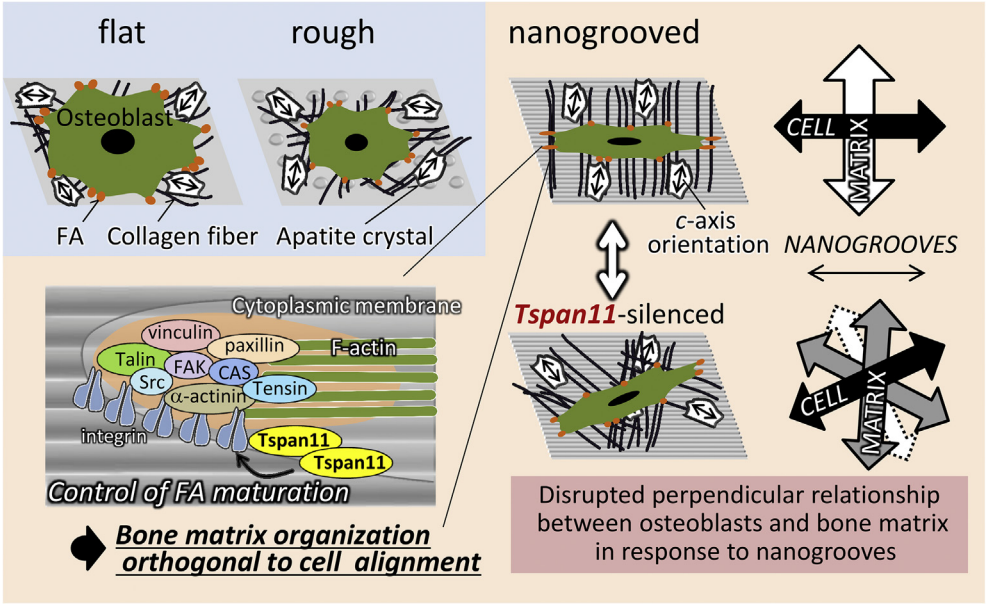

Fig. 6. Schematic illustration of the osteoblast response to surface topography. The osteoblasts enlarged with an abundance of FAs in response to a flat surface, and the osteoblasts on the rough surface occupied a smaller area; in both cases, the bone matrix showed non-directional structure. On the other hand, the osteoblasts elongated along nanogrooves with fibrillar FA maturation mediated by *Tspan11*, which was accompanied with bone matrix formation oriented orthogonal to cell alignment. FA, focal adhesion.

results indicated that *Gpm6b*-mediated signaling is one of the regulatory pathways in osteoblast adhesion depending on the surface roughness.

4.3. Bone matrix organization orthogonal to cell alignment

Collagen matrices secreted by osteoblasts aligned on the nanogrooves were organized orthogonal to cell alignment (Fig. 3), which was consistent with our previous work [7]. This finding is contrary to the general theory of parallel ECM formation, which has been supported by related studies [6,8–10]. Such parallel matrix organization has been considered to be derived from cellular contraction force [23] and collagen secretion processes involving fiber assembly in the extracellular space [24]. These proposed mechanisms involve cell–matrix adhesion molecule-mediated processes. Our present data suggested unique FA supermaturation specifically on the nanogrooved surface (Fig. 2), indicating that the bone matrix formation orthogonal to osteoblast alignment is possibly mediated by FA function. FAs exert multiple functions depending on their maturation; FAs can transform into fibrillar FAs that can modify the structure and rigidity of the ECM, contributing to tissue remodeling and repair [25]. Furthermore, contraction force is exerted in parallel to the direction of FA elongation, whereas round-shaped FAs can disperse the stress in an isotropic direction [26]. Anisotropic elongated FAs consist of assembled integrin molecules which possess a straight state, in which the molecules are less stable [27,28]. Taken together, the elongated FAs confined by the nanogrooved structure were more unstable than circularly spreading FAs. The bone matrix organized orthogonal to cell alignment likely provides sufficient space for isotropic FA formation to promote mechanical stability.

4.4. Role of Tspan11 in cell alignment and bone matrix organization

Microarray analysis revealed seven common genes (*Gm22519*, *Gm11115*, *Scarna10*, *A830039N20Rik*, *Tspan11*, *Gm22788*, and *Ifitm1*) significantly upregulated and seven genes (*9930111J21Rik2*, *Gm22642*, *Sdpr*, *Hbegf*, *Fam124a*, *Hist1h2aa*, and *Mir383*) downregulated in osteoblasts aligned on the nanogrooved surface compared with the other two types of surface structures (Fig. 4). Among these genes, we focused on the function of *Tspan11* because the tetraspanin family genes contribute to the regulation of cell adhesion signaling [29]. The degree of cell alignment was significantly decreased in *Tspan11*-silenced osteoblasts compared with osteoblasts transfected with the control siRNA (Fig. 5A). The tetraspanin family mediates cell adhesion processes via formation of tetraspanin-enriched microdomains (TEMs), which serve as structural and functional units in the plasma membrane [30]. The role of tetraspanins has been reported in regulation of adhesion, migration and metastasis procedure in other types of cells [31]. It is interesting that *Tspan11* silencing decreased the level of bone matrix organization perpendicular to cells, into more randomized directions (Fig. 5B). *Tspan11* silencing disrupted the perpendicular relationship between osteoblast alignment and cell-produced collagen matrix, as evidenced by the quantitative comparison of disruption efficiency of *Tspan11* silencing on the preferred orientation of cells and bone matrix organization (Fig. 5C). Moreover, *Tspan11* silencing significantly disrupted FA maturation along the nanogrooves as well as cell alignment (Fig. 5D). These results indicated that *Tspan11*-silenced osteoblasts failed to organize highly aligned morphology along nanogrooves with impaired FA maturation, and the alignment of collagen matrix perpendicular to cell alignment was further disrupted. The obtained results revealed the molecular association between FA structure and bone matrix orientation regulated by *Tspan11* (Fig. 6). The regulatory mechanism in the orthogonal organization of bone matrix proposed here is a specifically activated pathway in the limited environment with nanometer-scale patterning; the molecular mechanism determining the matrix orientation depending on the spacing size can exist. The present finding revealed the specific surface patterning obtained by a laser-induced self-organization process realized the orthogonal arrangement of bone matrix facilitated by FA assembly. A comprehensive research involving a wide range of surface topography with patterning from nanometer-to micrometer-scales is now in progress to clarify the spacing patterns critical for determining FA-mediated bone matrix organization.

5. Conclusion

It is commonly accepted that ECM orientation follows the cellular alignment; however, we demonstrated the abnormal arrangement of bone matrix orthogonal to osteoblast arrangement using a nanoscale grooved biomaterial surface. Notably, the discovery was associated with fibrillar FA formation along the nanogrooves. The comprehensive gene expression analysis revealed that the integrin clustering mediated by *Tspan11* determines the alignment of bone matrix architecture orthogonal to cell alignment. Our findings offer new strategies to realize the ideal microstructure of bone tissue as well as provide molecular

mechanisms for texture formation in biological systems.

Declarations of interest

None.

Author contributions

TY. N. designed the study. K. K., TF. N., and H. S. carried out the preparation of the substrates. Y. N. carried out the cell experiment. Y. N., A. M., and TY. N. interpreted the data. Y. N. and A. M. drafted the manuscript. TY. N. revised manuscript content. All authors contributed to discussion of the results.

Data availability

The raw and processed data required to reproduce these findings are available to download from https://data.mendeley.com/submissions/ees/edit/tp5hc6yrfg?submission_id=BIOMAT_76968&token=e64ade56-b374-43e1-bd13-53ebe618337d.

Acknowledgments

This work was supported by Grants-in-Aid for Scientific Research (S) (grant number 25220912, 18H05254), Challenging Research (Pioneering) (grant number 17H06224), and Grants-in-Aid for Young Scientists (A) (grant number 17H04955) from the Japan Society for Promotion of Science. The funders had no role in experiment planning, data collection and analysis as well as decision to publish.

References

[1] W.J. Landis, The strength of a calcified tissue depends in part on the molecular structure and organization of its constituent mineral crystals in their organic matrix, Bone 16 (1995) 533–544, https://doi.org/10.1016/8756-3282(95)00076-P.
[2] T. Nakano, K. Kaibara, Y. Tabata, N. Nagata, S. Enomoto, E. Marukawa, Y. Umakoshi, Unique alignment and texture of biological apatite crystallites in typical calcified tissues analyzed by microbeam x-ray diffractometer system, Bone 31 (2002) 479–487, https://doi.org/10.1016/S8756-3282(02)00850-5.
[3] T. Nakano, K. Kaibara, T. Ishimoto, Y. Tabata, Y. Umakoshi, Biological apatite (BAp) crystallographic orientation and texture as a new index for assessing the microstructure and function of bone regenerated by tissue engineering, Bone 51 (2012) 741–747, https://doi.org/10.1016/j.bone.2012.07.003.
[4] A. Matsugaki, G. Aramoto, T. Nakano, The alignment of MC3T3-E1 osteoblasts on steps of slip traces introduced by dislocation motion, Biomaterials 33 (2012) 7327–7335, https://doi.org/10.1016/j.biomaterials.2012.06.022.
[5] A. Matsugaki, N. Fujiwara, T. Nakano, Continuous cyclic stretch induces osteoblast alignment and formation of anisotropic collagen fiber matrix, Acta Biomater. 9 (2013) 7227–7235, https://doi.org/10.1016/j.actbio.2013.03.015.
[6] A. Matsugaki, Y. Isobe, T. Saku, T. Nakano, Quantitative regulation of bone-mimetic, oriented collagen/apatite matrix structure depends on the degree of osteoblast alignment on oriented collagen substrates, J. Biomed. Mater. Res. A 103 (2015) 489–499, https://doi.org/10.1002/jbm.a.35189.
[7] A. Matsugaki, G. Aramoto, T. Ninomiya, H. Sawada, S. Hata, T. Nakano, Abnormal arrangement of a collagen/apatite extracellular matrix orthogonal to osteoblast alignment is constructed by a nanoscale periodic surface structure, Biomaterials 37 (2015) 134–143, https://doi.org/10.1016/j.biomaterials.2014.10.025.
[8] J.H.C. Wang, F. Jia, T.W. Gilbert, S.L.Y. Woo, Cell orientation determines the alignment of cell-produced collagenous matrix, J. Biomech. 36 (2003) 97–102, https://doi.org/10.1016/S0021-9290(02)00233-6.
[9] S.J. Jones, A. Boyde, J.B. Pawley, Osteoblasts and collagen orientation, Cell Tissue Res. 159 (1975) 73–80, https://doi.org/10.1007/BF00231996.
[10] L. Wu, L.A. Lee, Z. Niu, S. Ghoshroy, Q. Wang, Visualizing cell extracellular matrix (ECM) deposited by cells cultured on aligned bacteriophage M13 thin films, Langmuir 27 (2011) 9490–9496, https://doi.org/10.1021/la201580v.
[11] I.D. Campbell, M.J. Humphries, Integrin structure, activation, and interactions, Cold Spring Harb. Perspect. Biol. 3 (2011) a004994, https://doi.org/10.1101/cshperspect.a004994.
[12] R. Changede, M. Sheetz, Integrin and cadherin clusters: a robust way to organize adhesions for cell mechanics, Bioessays 39 (2017) 1–12, https://doi.org/10.1002/bies.201600123.
[13] B.Z. Katz, E. Zamir, A. Bershadsky, Z. Kam, K.M. Yamada, B. Geiger, Physical state of the extracellular matrix regulates the structure and molecular composition of cell-matrix adhesions, Mol. Biol. Cell 11 (2000) 1047–1060, https://doi.org/10.1091/mbc.11.3.1047.
[14] A. Umeno, H. Kotani, M. Iwasaka, S. Ueno, Quantification of adherent cell orientation and morphology under strong magnetic fields, IEEE Trans. Magn. 37 (2001) 2909–2911, https://doi.org/10.1109/20.951344.
[15] M. Janko, P. Davydovskaya, M. Bauer, A. Zink, R.W. Stark, Anisotropic Raman scattering in collagen bundles, Opt. Lett. 35 (2010) 2765–2767, https://doi.org/10.1364/OL.35.002765 doi.org/.
[16] J. Bonse, J. Krüger, S. Höhm, A. Rosenfeld, Femtosecond laser-induced periodic surface structures, J. Laser Appl. 24 (2012) 042006, , https://doi.org/10.2351/1.4712658.
[17] M.J. Dalby, N. Gadegaard, M.O. Riehle, C.D.W. Wilkinson, A.S.G. Curtis, Investigating filopodia sensing using arrays of defined nano-pits down to 35 nm diameter in size, Int. J. Biochem. Cell Biol. 36 (2004) 2015–2025, https://doi.org/10.1016/j.biocel.2004.03.001.
[18] R. Lutz, K. Pataky, N. Gadhari, M. Marelli, J. Brugger, M. Chiquet, Nano-stenciled RGD-gold patterns that inhibit focal contact maturation induce lamellipodia formation in fibroblasts, PLoS One 6 (2011) e25459, , https://doi.org/10.1371/journal.pone.0025459.
[19] N.Q. Balaban, U.S. Schwarz, D. Riveline, P. Goichberg, G. Tzur, I. Sabanay, D. Mahalu, S. Safran, A. Bershadsky, L. Addadi, B. Geiger, Force and focal adhesion assembly: a close relationship studied using elastic micropatterned substrates, Nat. Cell Biol. 3 (2001) 466–472, https://doi.org/10.1038/35074532.
[20] C.F. Natale, M. Ventre, P.A. Netti, Tuning the material-cytoskeleton crosstalk via nanoconfinement of focal adhesions, Biomaterials 35 (2014) 2743–2751, https://doi.org/10.1016/j.biomaterials.2013.12.023.
[21] B. Baharloo, M. Textor, D.M. Brunette, Substratum roughness alters the growth, area, and focal adhesions of epithelial cells, and their proximity to titanium surfaces, J. Biomed. Mater. Res. A 74 (2005) 12–22, https://doi.org/10.1002/jbm.a.30321.
[22] K. Drabek, J. Van De Peppel, M. Eijken, J.P.T.M. Van Leeuwen, GPM6B regulates osteoblast function and induction of mineralization by controlling cytoskeleton and matrix vesicle release, J. Bone Miner. Res. 26 (2011) 2045–2051, https://doi.org/10.1002/jbmr.435.
[23] D. Karamichos, N. Lakshman, W.M. Petroll, Regulation of corneal fibroblast morphology and collagen reorganization by extracellular matrix mechanical properties, Investig. Ophthalmol. Vis. Sci. 48 (2007) 5030–5037, https://doi.org/10.1167/iovs.07-0443.
[24] E.G. Canty, Y. Lu, R.S. Meadows, M.K. Shaw, D.F. Holmes, K.E. Kadler, Coalignment of plasma membrane channels and protrusions (fibropositors) specifies the parallelism of tendon, J. Cell Biol. 165 (2004) 553–563, https://doi.org/10.1083/jcb.200312071.
[25] G.J. Goreczny, I.J. Forsythe, C.E. Turner, Hic-5 regulates fibrillar adhesion formation to control tumor extracellular matrix remodeling through interaction with tensin1, Oncogene (2018) 1–15, https://doi.org/10.1038/s41388-017-0074-2.
[26] H. Van Hoorn, R. Harkes, E.M. Spiesz, C. Storm, D. Van Noort, B. Ladoux, T. Schmidt, The nanoscale architecture of force-bearing focal adhesions, Nano Lett. 14 (2014) 4257–4262, https://doi.org/10.1021/nl5008773.
[27] A. Pathak, V.S. Deshpande, R.M. McMeeking, A.G. Evans, The simulation of stress fibre and focal adhesion development in cells on patterned substrates, J. R. Soc. Interface 5 (2008) 507–524, https://doi.org/10.1098/rsif.2007.1182.
[28] C.J. McCleverty, R.C. Liddington, Engineered allosteric mutants of the integrin alphaM beta2 I domain: structural and functional studies, Biochem. J. 127 (2003) 121–127, https://doi.org/10.1042/BJ20021273.
[29] C. Boucheix, E. Rubinstein, Tetraspanins, Cell. Mol. Life Sci. 58 (2001) 1189–1205, https://doi.org/10.1007/PL00000933.
[30] M. Yáñez-Mó, O. Barreiro, M. Gordon-Alonso, M. Sala-Valdés, F. Sánchez-Madrid, Tetraspanin-enriched microdomains: a functional unit in cell plasma membranes, Trends Cell Biol. 19 (2009) 434–446, https://doi.org/10.1016/j.tcb.2009.06.004.
[31] X. Jiang, J. Zhang, Y. Huang, Tetraspanins in cell migration, Cell Adhes. Migrat. 9 (2015) 406–415, https://doi.org/10.1080/19336918.2015.1005465.